IEICE TRANS. COMMUN., VOL.E90–B, NO.9 SEPTEMBER 2007

PAPER Special Section on 2006 International Symposium on Antennas and Propagation

Investigation on Seasonal Water Area Change in Lake Sakata Based on POLSAR Image Analysis

Ryoichi SATO[†a)], ***Member***, **Yuki YAJIMA**[††], ***Student Member***, **Yoshio YAMAGUCHI**[†††], ***and*** **Hiroyoshi YAMADA**[†††], ***Members***

SUMMARY This paper examines seasonal change of the true water area of Lake "Sakata" by using Polarimetric Synthetic Aperture Radar (POLSAR) image analysis. The true water area includes not only the body of water but also the water area under emerged-plants and/or floating-leave plants in the lake. Statistical POLSAR image analysis is carried out for both X- and L-band data, based on the three-component scattering power decomposition method, where the decomposed components are surface scattering, double-bounce scattering and volume scattering components. From the results of the image analysis for the L-band POLSAR data acquired by Pi-SAR system, it is found that strong double-bounce scattering can be observed at the vicinity of the boundary region between water area and the surrounding emerged-plants area in early and middle summer. This phenomenon is an important factor for environmental monitoring. To verify the generating mechanism of the double-bounce scattering, the Finite-Difference Time-Domain (FDTD) polarimetric scattering analysis is also executed for a simplified boundary model, which simulates the local boundary region around the lake and consists of lots of vertical thin dielectric pillars on a perfect electric conductor (PEC) plate or on a PEC and dielectric hybrid plate. Taking into account the polarimetric feature of the double-bounce scattering obtained by both the FDTD and POLSAR image analyses, one can distinguish the actual water area from the bush of the emerged-plants around the lake, even when the water area is concealed by emerged-plants and/or floating-leave plants. Consequently, it is found that by using the proposed approach, one can estimate the true water area seasonal change for the lake and the surrounding wetland.

key words: *radar polarimetry, polarimetric synthetic aperture radar (POLSAR), scattering power decomposition, water area change, wetland monitoring*

1. Introduction

Lake "Sakata," located in Niigata city, Japan, is one of the most beautiful sand dune lakes. The arrivals of many waterfowls can be observed every winter. Marshes surrounding the lake provide a comfortable environment for the waterfowls. So the lake and the surrounding area have been registered as a Ramsar Convention site [1] since 1996.

Sakata is a freshwater lake formed within sand dunes, and the freshwater is supplied only from spring water of the dunes and rainwater. There is no inflow from rivers into the lake, as seen in Fig. 1. Hence, it is very important to monitor and investigate the seasonal changes of the water area and water level. So far, some investigations on the seasonal water area change and the related topics have been reported in Refs. [2]–[4]. For wide area water area survey, a method by analyzing aerial photographs has been utilized [4]. However, such investigation method depends on the weather, since fine aerial photographs cannot be taken in bad weather condition. Therefore, an alternative monitoring method, independent of the weather condition, is required.

In this paper, we investigate seasonal water area change of Lake Sakata by using Polarimetric Synthetic Aperture Radar (POLSAR) image analysis. POLSAR is based on microwave remote sensing technology, so it can work well under any weather condition. The classification method used here is based on the scattering power decomposition on physical scattering nature [5]–[7]. In the well-known three-component decomposition method [5], total scattering contribution is decomposed into three scattering mechanisms as surface scattering, double-bounce scattering and volume scattering. In our previous studies in Refs. [6], [7], Helix scattering power component is added as the fourth component to the three-component scattering model of Ref. [5] to take into account the co-pol and the cross-pol correlations which may appear in urban environment. However, for natural distributed target area as wetland, such fourth component becomes minor contribution. Hence, we utilize here the simpler three-component scattering model. By using the three-component decomposition scheme, we carry out statistical POLSAR image analysis for actual data (X- and L-band data), acquired by Pi-SAR (developed by JAXA and NICT, Japan). It is found from the decomposed results for early and middle summer that the double-bounce scattering can be observed not only at the vicinity of the boundary between the lake and the surrounding emerged-plants, but also at some points inside the emerged-plants area. This double-bounce scattering may be caused by right angle structures composed of many vertical stems of the emerged-plants and

Manuscript received December 26, 2006.
Manuscript revised April 14, 2007.

[†]The author is with the Faculty of Education and Human Sciences, Niigata University, Niigata-shi, 950-2181 Japan.
[††]The author is with the Graduate School of Science and Technology, Niigata University, Niigata-shi, 950-2181 Japan.
[†††]The authors are with the Department of Information Engineering, Niigata University, Niigata-shi, 950-2181 Japan.
a) E-mail: sator@ed.niigata-u.ac.jp

DOI: 10.1093/ietcom/e90–b.9.2369

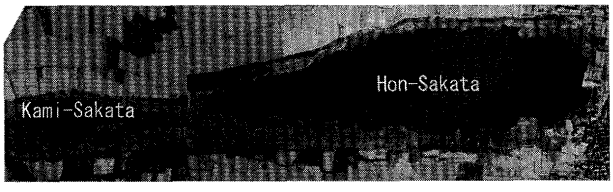

Fig. 1 Overview of Lake Sakata.

flat water surface, and it is utilized as a marker for estimating the actual water area of the lake. To the best knowledge of the authors, this is the first time to find out and introduce a useful marker for the distinction of the true water area of wetland in the field of classification and identification by POLSAR image analyses, although the methodlogy is known.

To verify the generating mechanism of the double-bounce scattering observed from the L-band images, by using the Finite-Difference Time-Domain (FDTD) method, polarimetric scattering analysis is also executed for a simplified boundary model, which simulates the local boundary region around the lake and consists of lots of vertical thin dielectric pillars on a perfect electric conductor (PEC) plate or on a PEC-dielectric hybrid plate. It is found from the FDTD analysis that similar strong double-bounce scattering is observed only for the former model with a PEC plate, that is, only for high water level case. Consequently, taking into account the polarimetric feature of the double-bounce scattering from the target region, one can distinguish the water area from the bush of the emerged-plants around the lake, even when the water area is concealed by emerged-plants and/or floating-leave plants. This cannot be accomplished by any means except for the present POLSAR technology.

Section 2 briefly introduces the scattering matrix and the corresponding covariance matrix in the present POLSAR image analysis. In Sect. 3, some decomposed results of the POLSAR image analysis and the detailed considerations are provided. In Sect. 4, the generating mechanism of the double-bounce scattering discussed in Sect. 3 is cleared by the FDTD polarimetric scattering analysis for simplified water-emergent boundary models.

2. POLSAR Image Analysis

To examine the seasonal water area change of the lake, we shall apply the scattered power decomposition method based on the three-component scattering model [5] to POLSAR data for Lake Sakata and the surrounding area. In this paper, let us simply show the decomposed procedure for the covariance matrix $[C]$, whose components are obtained by elements of Sinclair scattering matrix as

$$[S(HV)] = \begin{bmatrix} S_{HH} & S_{HV} \\ S_{VH} & S_{VV} \end{bmatrix} = \begin{bmatrix} a & c \\ c & b \end{bmatrix}, \quad (1)$$

where $S_{HV} = S_{VH} = c$ for back scattering case. The corresponding ensemble average covariance matrix $\langle[C]\rangle$ with the reflection symmetry condition $\langle S_{HH}S^*_{HV}\rangle \sim \langle S_{VV}S^*_{HV}\rangle \sim 0$ is given as

$$\langle[C]\rangle = \begin{bmatrix} \langle|a|^2\rangle & 0 & \langle ab^*\rangle \\ 0 & 2\langle|c|^2\rangle & 0 \\ \langle ba^*\rangle & 0 & \langle|b|^2\rangle \end{bmatrix} \quad (2)$$

$$= f_s\langle[C]\rangle_{surface} + f_d\langle[C]\rangle_{double} + f_v\langle[C]\rangle_{vol}, \quad (3)$$

where $\langle\cdot\rangle$ denotes the ensemble average in the data processing, $\langle[C]\rangle_{surface}$, $\langle[C]\rangle_{double}$ and $\langle[C]\rangle_{vol}$ are the covariance matrices for surface scattering, double-bounce scattering and volume scattering, respectively (See Fig. 2 and Appendix). Also, f_s, f_d and f_v are the unknown deterministic coefficients for each scattering component. The deterministic algorithm for the unknowns f_s, f_d, f_v are shown in Fig. 3. The present algorithm for the three-component scattering model is as same as that for the four-component scattering model of Refs. [6],[7] when the Helix scattering component f_c equals zero. According to the algorithm as in Fig. 3, by choosing the appropriate matrices $\langle[C]\rangle_{surface}$, $\langle[C]\rangle_{double}$, $\langle[C]\rangle_{vol}$, the total scattered power can be successfully decomposed into each scattering component, P_s, P_d, and P_v.

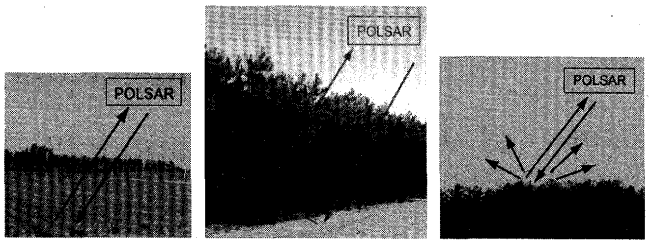

(a) P_s (b) P_d (c) P_v

Fig. 2 Three scattering component model. (a) Surface scattering (P_s), (b) double-bounce scattering (P_d), (c) volume scattering (P_v).

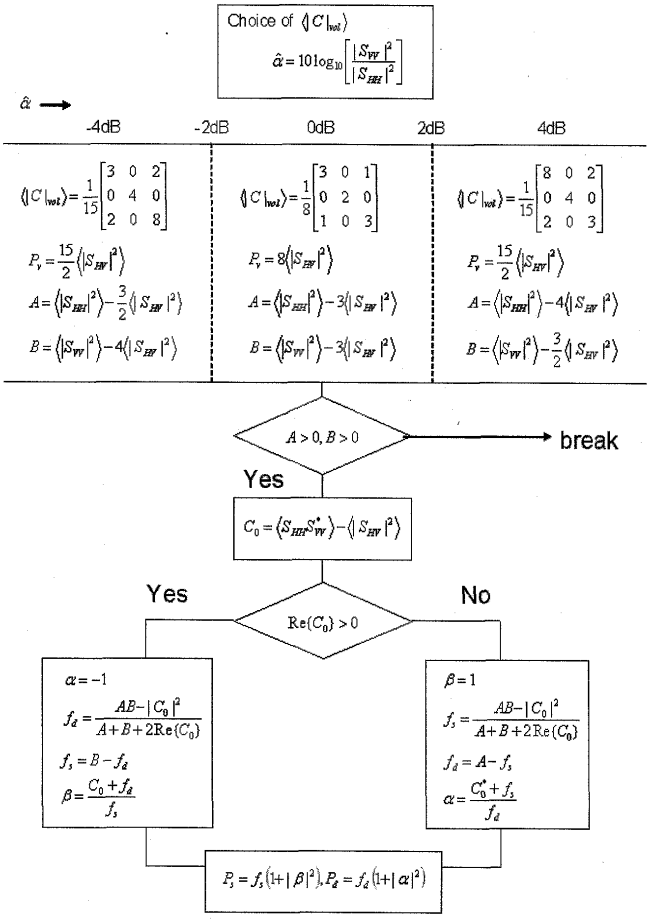

Fig. 3 A deterministic algorithm for the unknowns f_s, f_d, f_v [5], [6].

3. Results of POLSAR Analysis

Three scattering component decomposition method was applied to the POLSAR data around Lake Sakata acquired by Pi-SAR system, which is an airborne Polarimetric interferometric Synthetic Aperture Radar system developed by JAXA and NICT, Japan. Figure 4 shows the decomposed results for the POLSAR image data measured on June 13, 2002. Figure 4(a) is the result at X-band (9.55 GHz), and Fig. 4(b) is at L-band (1.27 GHz). The resolution of each pixel and the average size are 1.25 m by 1.25 m and 10 by 10 pixels for X-band, and 2.5 m by 2.5 m and 5 by 5 pixels for L-band, respectively. In the figures, the decomposed scattering powers are color-coded as follows. 1) Blue color is painted for surface scattering P_s, 2) Red is for double-bounce scattering P_d, and 3) Green is for volume scattering P_v. As seen in Fig. 4, the decomposed result for X-band has higher resolution than that for L-band on the whole. However, for the emerged-plants area around the water area, one can observe that the X-band image shows uniformly blue of surface scattering. This is due to the fact that the X-band wave cannot penetrate into the vegetation area, especially the emerged-plants area, so the scattering from the upper region (surface) of the emerged-plants is only observed. Hence, it may be unsuitable to survey the lower region under the emerged-plants. While, most of the L-band wave can penetrate into the emerged-plants, so that the L-band data may be suitable for estimating the actual water area of the lake and the surrounding wetland. Therefore, we will consider the polarimetric feature for the L-band images from now on.

Figure 5 shows the L-band color composite images around Kami-Sakata area. There are several red color spots

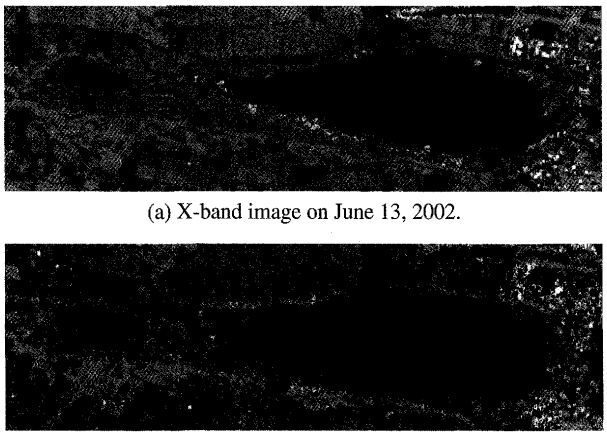

(a) X-band image on June 13, 2002.

(b) L-band image on June 13, 2002.

Fig. 4 Color composite images of Lake Sakata and the surrounding wetland area.

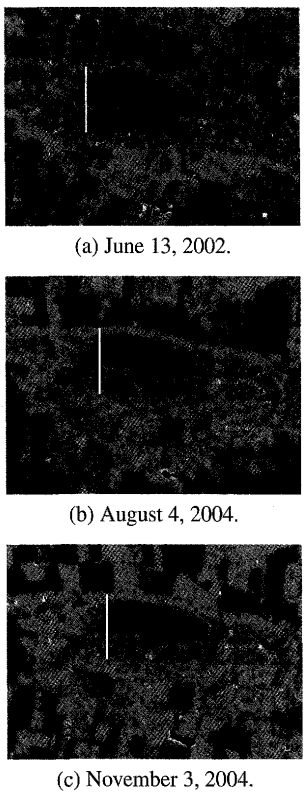

(a) June 13, 2002.

(b) August 4, 2004.

(c) November 3, 2004.

Fig. 5 Color composite images of Kami-Sakata area.

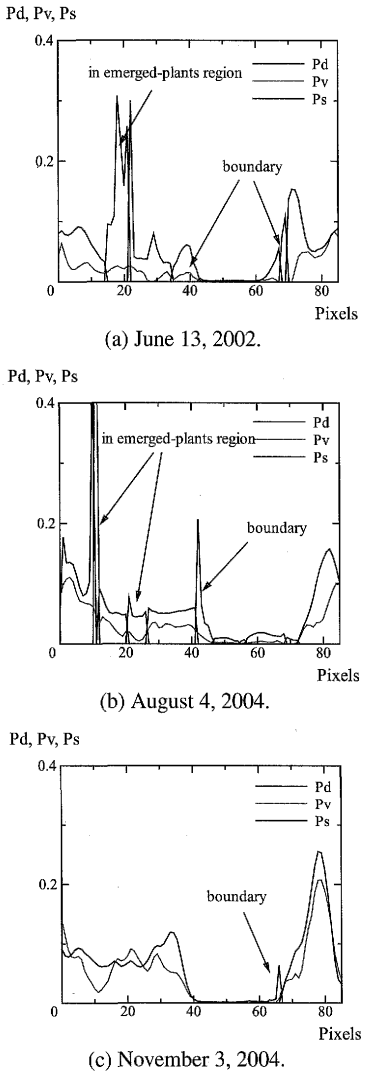

(a) June 13, 2002.

(b) August 4, 2004.

(c) November 3, 2004.

Fig. 6 Decomposed results along a transect in Kami-Sakata area.

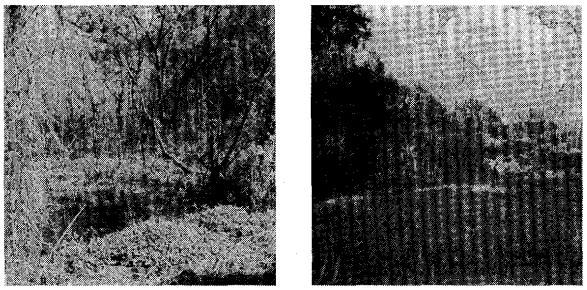

Fig. 7 Spring water pools in emerged-plant area around Kami-Sakata.

for P_d at the surrounding region of the lake in early summer (Fig. 5(a)), and in middle summer (Fig. 5(b)). Such red spots (double-bounce scattering) are generally caused by fine dihedral structures of man-made targets, whose all dimensions are large enough compared to wavelength [8]. For this case, the vertical stem of emerged-plants (reeds) and the water surface constitute dihedral corner reflector structures at the boundary of the lake, even though each emerged-plant is very thin (small) compared to the wavelength of the L-band wave. The dihedral structures may be finely constructed when the water level is high. For low water level case, fine dihedral structures are not made-up at the boundary. So the red color spot of the double-bounce scattering is hardly observed in autumn season of Fig. 5(c).

In Fig. 6, to check the existence of the red spots in detail, let us show the decomposed results along the transect in Fig. 5. From Figs. 6(a) and (b), one can observe the red spots not only at the water-emergent boundaries but also inside the emergent regions. The latter strong double-bounce scattering of the red spots may be caused by the existence of the spring water pools inside the emergent (See Fig. 7), that is, fine dihedral structures may be constructed by the water surface of the spring water pools and the emerged-plants. So far, it has been reported in Refs. [9], [10] that similar characteristic increasing radar responses can be observed from flooded rice regions even for C-band (5.3 GHz) satellite SAR images, although the polarimetric scattering feature has not been discussed in the analyses at all. In next section, to verify the assumed scenario for generating the double-bounce scattering, we will carry out the polarimetric scattering analysis for simplified water-emergent boundary models by using the Finite-Difference Time-Domain (FDTD) method [11].

4. FDTD Polarimetric Scattering Analysis

As depicted in Fig. 8, we will consider polarimetric scattering problem when H (horizontal) or V (vertical) linear polarized plane wave impinges on a simplified boundary model, which simulates the local boundary region around the lake and consists of lots of vertical thin dielectric pillars on a perfect electric conductor (PEC) plate (Model (a))or on a PEC and dielectric hybrid plate (Model (b)). Model (a) simulates the vertical stems of the emerged-plants on water surface where the water level is assumed as high, and Model (b) is

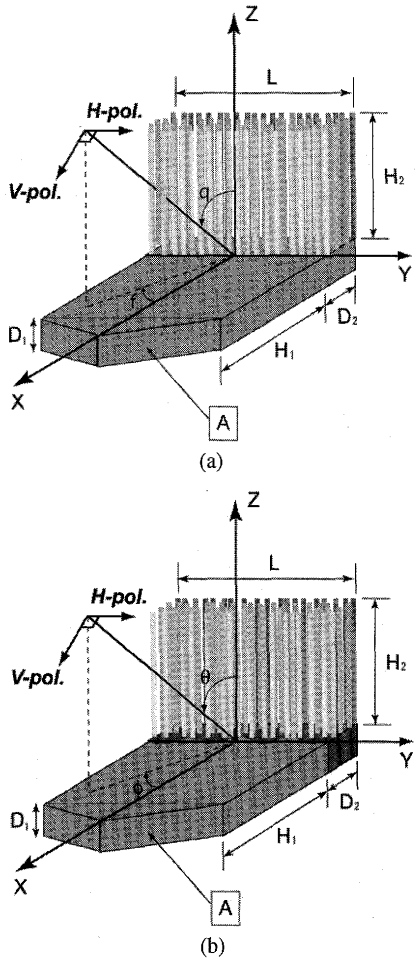

Fig. 8 Geometry of the problem (θ: look angle, ϕ: squint angle). (a) Vertical dielectric pillars on PEC plate, (b) vertical dielectric pillars on PEC-dielectric hybrid plate.

for low water level case that the emerged-plants are emerged near the boundary between soil ground and water area.

Here, the FDTD method [11] is utilized to obtain the scattering matrix for the models. The incident and squint angles are $\theta = \theta_i = 45^o$ and $\phi = \phi_i = 0^o$, respectively. Each dimension size of the scatterer is $L = 10.17\lambda$ (2.40 m), $H_1 = 5.93\lambda$ (1.40 m), $D_1 = 2.54\lambda$ (0.60 m) and $D_2 = 3.60\lambda$ (0.85 m) at 1.27 GHz frequency, where a compensated trigonal part A is added to reduce the unnecessary back scattering from the horizontal edge of the front side. At 1.27 GHz, the complex relative permittivity ε^*_{r1} for the thin dielectric pillars is set as $2.0 - j0.05$, and ε^*_{r2} for the dielectric part of the base plate in model (b) is $5.0 - j0.1$. Three hundreds of thin square dielectric pillars are randomly located on a part of the base plate ($D_2 \times L$ area). The cross section of each pillar is 0.01 m × 0.01 m. The other fundamental parameters of the FDTD simulation used here are shown in Table 1.

In this paper, to evaluate statistical polarimetric scattering feature as actual POLSAR image analysis, the vertical pillars are randomly set on the plate, and the ensemble average processing is carried out for random 25 distributed patterns (snapshots) of the pillars. The results of the statistical evaluation are shown in Table 2, where H_2 is relatively

Table 1 Parameters in FDTD analysis.

Analytical region	350×350×350 cells
Cubic cell size Δ	0.01 m
Time step Δt	1.925×10^{-11} s
Incident pulse	Lowpass Gaussian pulse
Absorbing boundary condition	Mur 2nd

Table 2 FDTD statistical evaluation results of the polarimetric scattering from the boundary models.

Scattering component	Model (a)	Model (b)
P_s/P_t	0.17568	0.83320
P_d/P_t	0.81015	0.15831
P_v/P_t	0.01417	0.00849

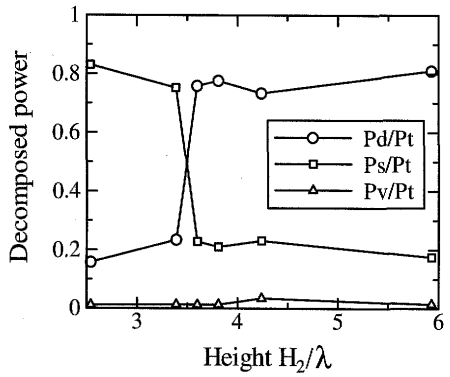

Fig. 9 Pillars' height dependency of the decomposed scattering power obtained by FDTD statistical analysis.

high as 5.93λ (1.40 m). In the table, each decomposed power is normalized by the total power $P_t(= P_s + P_d + P_v)$. It is observed from the result for Model (a) that the dominant scattering contribution is P_d for the high water level case. While, for the low water level case of Model (b), the strong surface scattering is generated at the boundary between PEC (water) and dielectric (soil) parts.

To make the generating mechanism of the double-bounce scattering clearer, we further examine the pillars' height dependency for the high water level case of Model (a). Figure 9 shows the pillars' height dependency of the normalized decomposed power for Model (a) obtained by the same statistical FDTD analysis. It is observed from the figure that when the height is relatively high over 3.5λ, the double-bounce scattering P_d is much greater than the other scattering contributions. Whereas, in proportion to the decrease of the height, P_d becomes small. For the case that the height is smaller than about 3.5 λ, the surface scattering P_s, which may be generated at the upper parts (surface) of the pillars, becomes dominant contribution, instead of P_d. Also, for this model, the volume scattering P_v is evaluated to be very small compared to the other components.

Taking into account the results of the above statistical FDTD polarimetric scattering analyses, the following conclusion may be obtained.

- Strong P_d can be observed when water level and height of plants are both enough high. (The height of emerged-plants is generally enough high compared to L-band wavelength.)
- P_s is the dominant factor rather than P_d for low water level case and/or for short height plants case (less than about 3.5λ).

5. Concluding Remarks

Seasonal change of the water area of Lake Sakata has been investigated by using POLSAR image analysis. Statistical POLSAR image analysis has been carried out for L-band data, based on a three-component scattering power decomposition method. Taking into account the polarimetric feature of the double-bounce scattering from the target region, one has been able to distinguish the water area from the bush of the emerged-plants around the lake when the water level is relatively high. This specific double-bounce scattering is considered as a new useful marker for the distinction of the true water area of wetland.

To verify the generating mechanism of the double-bounce scattering, the FDTD statistical polarimetric scattering analysis has also been executed for simplified water-ground boundary models, and the similar polarimetric feature for the double-bounce scattering has been observed from the simulation for high water level case, when the plants model is higher than about 3.5λ at L-band frequency.

Therefore, by extracting the double-bounce scattering contribution from the entire image, one can easily classify the true water area around the lake. This classification procedure can be suitable even for finding out the small spring water pools inside the emerged-plants area around the lake when most of the water area of the pool is concealed by the emerged-plants and/or floating-leave plants. This approach may also present us a helpful tool for water area observation of vast and severe wetlands where one can not carry out on-site inspections for grasping the situation.

As a future development, we will consider to apply the present polarimetric power decomposition method for monitoring rice crop growth, since the generating mechanism of the double-bounce scattering from the water-emergent boundary is similar to that from flooded rice regions [9], [10].

Acknowledgments

The authors express their sincere appreciations to Professor H. Fukuhara of Niigata University for helpful discussions, to JAXA and NICT, Japan, for providing valuable Pi-SAR image data around Lake Sakata, and to the anonymous reviewer for his useful comment. This research was partially supported by a Scientific Research Grant-In-Aid from JSPS (Japan Society for the Promotion of Science), Japan, and 2005 Niigata City Sakata Wetland Scientific Research Incentive Grant.

References

[1] Official Web site of the Ramsar Convention on Wetlands, http://www.ramsar.org/index.html
[2] M. Nonaka, R. Abe, and T. Kamura, "Nitrate movement through soil profile and groundwater pollution by nitrogen fertilizer in sand dune upland soil," Jpn. J. Soil Sci. Plant Nutr., vol.67, pp.633–639, 1996.
[3] H. Fukuhara, A. Kawakami, and T. Shimogaito, "Characteristics of nutrient dynamics in Lake Sagata, Japan, a shallow sand dune lake," Hydrobiologia, vol.506-509, pp.93–99, 2003.
[4] H. Fukuhara et al., "Limnological studies of lakes in Niigata prefecture X, changes in the area of emerged and floating-leaved plants, estimated by using aerial photographs, in Lake Sagata (Akatsuka, Niigata)," Memoirs of the Faculty of Education and Human Sciences, Niigata University, vol.1, no.1, pp.1–15, Sept. 1998.
[5] A. Freeman and S.L. Durden, "A three-component scattering model for polarimetric SAR data," IEEE Trans. Geosci. Remote Sens., vol.36, no.3, pp.963–973, May 1998.
[6] Y. Yamaguchi, T. Moriyama, M. Ishido, and H. Yamada, "Four-component scattering model for polarimetric SAR image decomposition," IEEE Trans. Geosci. Remote Sens., vol.43, no.8, pp.1699–1706, Aug. 2005.
[7] Y. Yamaguchi, Y. Yajima, and H. Yamada, "A four-component decomposition of POLSAR images based on the coherency matrix," IEEE Geosci. Remote Sens. Lett., vol.3, no.3, pp.292–296, July 2006.
[8] K. Hayashi, R. Sato, Y. Yamaguch, and H. Yamada, "Polarimetric scattering analysis for a finite dihedral corner reflector," IEICE Trans. Commun., vol.E89-B, no.1, pp.191–195, Jan. 2006.
[9] T. Kurosu, M. Fujita, and K. Chiba, "Monitoring of rice crop growth from space using the ERS-1 C-band SAR," IEEE Trans. Geosci. Remote Sens., vol.33, no.4, pp.1092–1096, July 1995.
[10] T.L. Toan, F. Ribbes, L.-F. Wang, N. Floury, K.-H. Ding, J.A. Kong, M. Fujita, and T. Kurosu, "Rice crop mapping and monitoring using the ERS-1 data based on experiment and modeling results," IEEE Trans. Geosci. Remote Sens., vol.35, no.1, pp.41–56, Jan. 1997.
[11] A. Taflove and S.C. Hagness, Computational Electrodynamics, 2nd ed., Artech House, 2000.

Appendix: Covariance Matrix for Three-Component Scattering Model

In the procedure of the power decomposition method based on three-component scattering model [5], the following covariance matrix is utilized for each scattering component.

The covariance matrices for double-bounce scattering and surface scattering are modeled as

$$\langle [C] \rangle_{double} = \begin{bmatrix} 1 & 0 & \alpha^* \\ 0 & 0 & 0 \\ \alpha & 0 & |\alpha|^2 \end{bmatrix} \quad (A\cdot 1)$$

and

$$\langle [C] \rangle_{surface} = \begin{bmatrix} |\beta|^2 & 0 & \beta \\ 0 & 0 & 0 \\ \beta^* & 0 & 1 \end{bmatrix}, \quad (A\cdot 2)$$

respectively, where α and β are unknown parameters to be determined in the deterministic algorithm of Fig. 3.

Volume scattering is considered as a sum of randomly scattered waves from vegetations. Here, a randomly oriented dipole model is employed, where the model simulates actual forests, tree trunk, branch, and so on. Therefore, the covariance matrix for volume scattering is dependent on the dominant orientation of the dipole set [6]. When vertical dipole is dominant rather than horizontal one, then the covariance matrix becomes

$$\langle [C] \rangle_{vol} = \frac{1}{15} \begin{bmatrix} 8 & 0 & 2 \\ 0 & 4 & 0 \\ 2 & 0 & 3 \end{bmatrix}. \quad (A\cdot 3)$$

While, for the horizontal dipole dominant case,

$$\langle [C] \rangle_{vol} = \frac{1}{15} \begin{bmatrix} 3 & 0 & 2 \\ 0 & 4 & 0 \\ 2 & 0 & 8 \end{bmatrix}. \quad (A\cdot 4)$$

Also, when the scatterers in the target vegetation area is quite randomly oriented about the radar look direction, that is, there is no dominant orientation in the dipole set, the covariance matrix can be described as

$$\langle [C] \rangle_{vol} = \frac{1}{8} \begin{bmatrix} 3 & 0 & 1 \\ 0 & 2 & 0 \\ 1 & 0 & 3 \end{bmatrix}. \quad (A\cdot 5)$$

By using the algorithm of Fig. 3, the appropriate covariance matrix for volume scattering can be selected from the above three candinates (A·3)–(A·5).

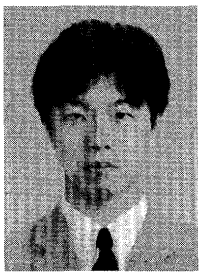

Ryoichi Sato received the B.S., M.S. and Ph.D. degrees in electrical engineering from Chuo University, Tokyo, Japan, in 1992, 1994 and 1997, respectively. Since April 1997, he has been with the Faculty of Education and Human Sciences, Niigata University, Japan, where he is currently an associate professor. In 2002, he was a Research Scholar at Polytechnic University, Brooklyn, NY. His current research interests are electromagnetic wave propagation, scattering and diffraction, and radar polarimetry. Dr. Sato is a member of IEEE.

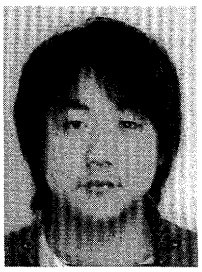

Yuki Yajima was born in Niigata, Japan, on Feburary 18, 1981. He received the B.E. degree in information engineering, from Niigata University, Niigata, Japan, in 2005. He is currently persuing the M.E. degree at Niigata University. He is engaged in POLSAR image analysis.

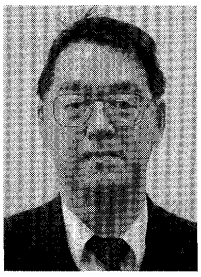

Yoshio Yamaguchi received the B.E. degree in electronics engineering from Niigata University in 1976, and M.E. and Dr. Eng. degrees from Tokyo Institute Technology in 1978 and 1983, respectively. In 1988, he joined the Faculty of Engineering, Niigata University, where he is a professor. From 1988 to 1989, he was a Research Associate at University of Illinois at Chicago. His interests are in the field of propagation characteristics of electromagnetic waves in lossy medium, radar polarimetry, microwave remote sensing and imaging. Dr. Yamaguchi is a Fellow of IEEE.

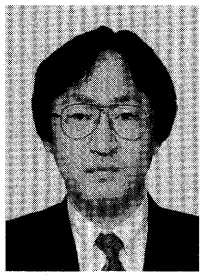

Hiroyoshi Yamada received the B.E., M.E., and Dr. Eng. degrees from Hokkaido University, Sapporo, Japan, in 1988, 1990 and 1993, respectively, all in electronic engineering. In 1993, he joined the Faculty of Engineering, Niigata University, where he is an associate professor. From 2000 to 2001, he was a Visiting Scientist at Jet Propulsion Laboratory, California Institute of Technology, Pasadena. His current interests involve in the field of array signal processing, radar polarimetry and interferometry, microwave remote sensing and imaging. Dr. Yamada is a member of IEEE.